

On the mechanisms of the corrosion of weathering steel by SO₂ in laboratory studies: influence of the environmental parameters

J. F. Marco¹

© Springer International Publishing Switzerland 2017

Abstract We report here on the mechanisms underlying the corrosion of weathering steel in accelerated laboratory tests using artificially polluted SO₂-atmospheres. The role of corrosion parameters such as the SO₂ concentration, the exposure time, the relative humidity and temperature of the environment are discussed in detail. Through the extensive use of Mössbauer spectroscopy in both its transmission and electron detection modes, as well as with the help of other analysis techniques, the characterization of the different corrosion products at the various stages of the corrosion process has been carried out. The results complement the data obtained in field studies and help to understand the mechanisms involved in this complex phenomenon.

Keywords Weathering steel · Corrosion · SO₂ · Protective patina · Environmental parameters · Mössbauer spectroscopy

1 Introduction

Except for a very few exceptions, such as gold, metals are not found in their native form in nature. If isolated, they tend to revert to their oxidized variants under ambient conditions. Metallic corrosion can be defined, thus, as the degradation that metals and metallic materials suffer when exposed to the environment [1]. The economic costs of corrosion are huge as they not only comprise the direct costs derived from the repair or replacement of the degraded materials but also all the indirect costs associated to these repairs or replacements:

This article is part of the Topical Collection on *Proceedings of the 15th Latin American Conference on the Applications of the Mössbauer Effect (LACAME 2016), 13-18 November 2016, Panama City, Panama*
Edited by Juan A. Jaén

✉ J. F. Marco
jfmarco@iqfr.csic.es

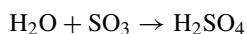
¹ Instituto de Química Física “Rocasolano”, CSIC, Serrano 119, 28006 Madrid, Spain

labour costs, lack of service during long periods, insurance, etc. Some recent studies quantify these costs to amount up to 3.4% of the Gross Domestic Product at a global level in 2013 [2].

We will focus in this work on atmospheric corrosion, i.e., that occurring under the conditions provided by particular combinations of the composition of the gaseous atmosphere in our immediate environment and we will not talk about other important types of corrosion such as those taking place, for example, under immersion conditions, as it is the case of ships or bridges, underneath the soil, as the one prevalent in materials for water supply and sewage or oil extraction, etc.

In the case of atmospheric corrosion, relative humidity, the presence of certain pollutants and the exposure time are factors of crucial importance. Below a certain “critical relative humidity” corrosion does not occur. Some pollutants have a very important accelerant and deleterious effect. Among these atmospheric pollutants sulphur dioxide (SO₂) is of paramount importance. The sources of atmospheric SO₂ can be both natural and anthropogenic. The natural SO₂ emissions are mainly related to volcano eruptions while anthropogenic emissions are basically due to burning coal and petrol. The anthropogenic emissions peaked at the 70s-80s of the past century and then decreased noticeably in USA and Europe due to a more strict environmental control and the use of better quality fuels for road transportation. However, in recent years, since 2000 on, the SO₂ emissions started increasing significantly in other parts of the world, particularly in East Asia [3]. The role of SO₂ as atmospheric pollutant and then as corrosion promoter is, thus, still relevant.

In general SO₂ is selectively adsorbed on metal surfaces. Under humid conditions these metal surfaces catalyse SO₂ to sulphur trioxide (SO₃) promoting the formation of sulphuric acid according to the reaction:



The corrosion of metal surfaces takes place subsequently under these acidic conditions.

In any case it is evident that the understanding of any corrosion mechanism implies the most accurate identification possible of the corrosion products formed at the different stages of the corrosion process. So, although the Pourbaix diagrams [4] tell us about what compounds can be formed under a particular set of conditions (that is they inform about what is thermodynamically possible) they do not tell what is actually occurring. Hence, in the case of iron-containing materials, which are most extended and whose economical relevance is undeniable, is where Mössbauer spectroscopy becomes a really powerful tool in corrosion research.

The advantages of Mössbauer spectroscopy in corrosion studies have been summarized long ago but [5–9] it is worth to repeat them here:

- The large database of Mössbauer parameters of iron oxides, oxyhydroxides (including nanosized phases), sulphates, green rusts, etc., facilitates their identification within a corrosion layer.
- Besides this qualitative analysis, quantitative analysis is also possible, i.e., the relative concentrations of the various corrosion products can be determined.
- It allows the study of thin films by detection of resonant electrons. Therefore, by combining both transmission and electron detection modes, relevant information spanning from the very initial corrosion stages until much further ones can be obtained.
- It allows the study “in situ” of corrosion processes in aggressive media.
- It allows the study of corrosion processes occurring beneath an inert coating by detecting the appropriate resonant radiation.



Fig. 1 Santa Mónica parish in Rivas-Vaciamadrid (Spain) built with Cor-Ten steel. Note the spectacular colour of the patina formed on the steel surface (photo taken by the author)

We will focus in this paper on the corrosion of weathering steels in artificially polluted SO_2 atmospheres. Weathering steels, also called low-alloy steels, are steels that have in their composition small amounts (less than 0.5%) of Cu, Mn and Cr. They are also known as structural steels and are usually employed in buildings, bridges, open-air sculptures etc. without protective paintings or coatings since they show a remarkable resistance to atmospheric corrosion due to the formation of a self-protective patina of corrosion products. This patina has a very attractive appearance (Fig. 1) and sometimes it has been described as having a colour as only Nature can produce, similar to those found in minerals and forests [10]. It has been reported that the presence of SO_2 helps in the development of such patina [11]. The elucidation of its protective nature has been the matter of large number of investigations and its composition has been subjected to much speculation [12–14]. Mössbauer spectroscopy has played a major role in such elucidation [15]. We report here in a quite systematic laboratory study that we have conducted to understand the role of parameters such as SO_2 concentration, relative humidity, succession of wet-dry cycles or exposure time in the composition of the above-mentioned patina.

2 Experimental

2.1 Corrosive media and conditions

In all our studies we have simulated the SO_2 -polluted atmospheres following a procedure described by Evans [16]. According to this procedure, the SO_2 -polluted atmosphere is generated according to the reaction:



The concentration of SO₂ is controlled by the concentration of the K₂S₂O₅ solution while the relative humidity (rh) is controlled by the concentration of the H₂SO₄ solution. We have used different SO₂ concentrations: 0.001%, 0.008%, 0.04% and 0.22% by vol. The solutions are placed in the bottom of a desiccator while the materials exposed to the corrosive atmosphere are placed in a glass grid above the solutions.

We have carried out to types of exposure conditions:

- *Constant relative humidity* (98%) for exposure times ranging from 0.5 hours to 72 hours
- *Wet-dry cycles*: up to 24 cycles with different duration of the wet and dry periods:
 - wet period: 6h, dry period: 18 h (henceforth, SW type cycle)
 - wet period: 18h, dry period: 6h (henceforth, LW type period)

The experiments were carried out at ambient temperature (25 °C) except for a particular set of exposures where the temperature of the dry period was raised to 40 °C.

2.2 Studied materials

We have studied the corrosion behaviour of pure iron (COMECA, Saint Cyr L'Ecole, France, maximum limit of C+P+Cu+Mn+Si impurities, 0.25%) and weathering steel (COR-TEN-B, Altos Hornos de Vizcaya, Spain, with chemical composition 0.17% C, 0.27% Si, <0.1% P, 0.018% S, 0.030% Cu, 0.52% Cr, <0.001% Ni, 0.07% Al and <0.02% V). In all the cases, coupons of 25 mm in diameter were polished with emery paper and alumina paste down to 0.3 μm until a mirror surface was obtained.

2.3 Characterization techniques

A range of analytical techniques was used to characterize the samples studied.

⁵⁷Fe Mössbauer spectroscopy was used in both transmission and electron detection modes (CEMS). In both cases, a conventional constant acceleration spectrometer with a ⁵⁷Co(Rh) source was used. The transmission experiments were carried out in a closed cycle He cryo-refrigerator [17] while for the CEMS measurements a parallel plate avalanche counter was used [18]. A home-made spherical analyser for Depth Selective CEMS (DCEMS) was used in a few particular cases. The velocity scale was calibrated using a 6 μm thick iron foil and the isomer shifts were referred to the centroid of the α-Fe spectrum at room temperature.

Scanning Electron Microscopy (SEM) images were recorded using an ISI microscope model DS-130 under an electron accelerating voltage of 20 kV.

X-ray Photoelectron Spectroscopy (XPS) data were recorded using a XPS system equipped with a three channeltrons CLAM2 analyser (VG) under a base pressure lower than 1 · 10⁻⁸ mbar, Al Kα radiation and a pass energy of 20 eV. The binding energies were referred to the C 1s carbon adventitious layer, which was set at 284.6 eV.

3 Results and discussion

3.1 Characteristic room temperature CEMS spectra

Under all the experimental corrosion conditions used, room temperature CEMS spectra recorded from the different corroded samples are the combination of, as much, six different

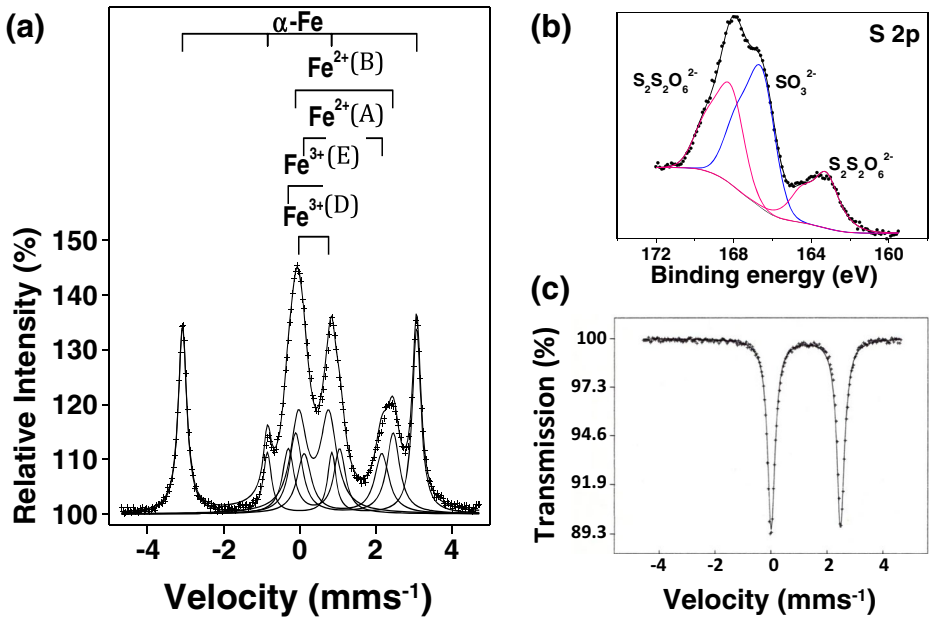


Fig. 2 **a** Room temperature CEMS spectrum recorded from a 3 nm thick ^{57}Fe layer after 15 min exposure to an atmosphere containing 0.04 vol% SO_2 and 98% rh. **b** S 2p XPS spectrum recorded from the sample whose CEMS spectrum is given in Fig. 2a. **c** Room temperature transmission Mössbauer spectrum recorded from $\text{FeSO}_3 \cdot 3\text{H}_2\text{O}$

Table 1 Room temperature Mössbauer parameters of the corrosion products

Species		$\delta(\text{mm s}^{-1})$	$\Delta(\text{mm s}^{-1})$	Assignment
Fe^{2+}	A	1.24	1.90	Fe^{2+} thiosulphate/tetrathionate
	B	1.27	2.54	$\text{FeSO}_3 \cdot 3\text{H}_2\text{O}$
	C	1.25	3.16	$\text{FeSO}_4 \cdot n\text{H}_2\text{O}$
Fe^{3+}	D	0.38	0.67	Spm goethite/lepidocrocite/amorphous oxyhydroxide/ferrihydrate
	E	0.38	1.08	amorphous oxyhydrox./ferrihydrate

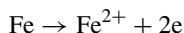
contributions: five doublets corresponding to different corrosion products plus the spectrum from the substrate. The relative areas of the different components depend on the SO_2 concentration, exposure time, relative humidity, type of wet-dry cycles or base material. Figure 2a shows one of these representative room temperature CEMS spectra recorded from a 3 nm thick ^{57}Fe thin film exposed for 15 min to an atmosphere having 0.04 vol% SO_2 and 98% rh [19]. Table 1 collects the Mössbauer parameters of the usual five contributions due to the corrosion products. In this type of experiments in SO_2 -polluted atmospheres, $\text{FeSO}_4 \cdot n\text{H}_2\text{O}$ appears only after exposure to a large number of wet-dry cycles and, usually, in small concentrations. This is why we have included this species in Table 1 but it is not shown in the corresponding spectrum on the left. Figure 2b shows the S 2p XPS spectrum recorded from the mentioned film. It contains three contributions: the one at 166.7 eV corresponds to

sulphite (SO_3^{2-}) species [19] while the contributions at 163.3 eV and 168.6 eV can correspond either to thiosulphate species [20] or a tetrathionate species [21]. Both species have two different kinds of sulphur present in its structure that are nicely resolved by XPS. We associate the sulphite species with doublet B due to $\text{FeSO}_3 \cdot 3\text{H}_2\text{O}$. This corrosion product was also detected in the X-ray powder diffraction patterns recorded from the rust. In order to know its Mössbauer parameters we synthesized this compound according to the procedure described in [22] and recorded its corresponding Mössbauer spectrum (Fig. 2c). The obtained parameters matched those of doublet B. The assignment of doublet A to a ferrous species was much more elusive and the use of XPS was of crucial importance to associate it to an Fe^{2+} thiosulphate/tetrathionate species. Regarding the parameters of the Fe^{3+} species, several compounds such as “amorphous ferric oxide”, superparamagnetic goethite, ferrihydrite or lepidocrocite could account for them [23–27]. As it is well known, the unequivocal identification of different Fe^{3+} oxyhydroxides from a room temperature Mössbauer spectrum is very difficult even more when superparamagnetic particles (as it is the case here) are present. In this situation, recording series of low temperature spectra becomes compulsory (*vide infra*).

3.2 Corrosion of weathering steels in simulated SO_2 -polluted atmospheres

3.2.1 Influence of SO_2 concentration

Figure 3 (left) shows the CEMS spectra recorded from weathering steel after three hours of exposure to atmospheres containing different SO_2 concentrations and 98% relative humidity. As it can be observed, in the lowest SO_2 concentration (0.008 in vol%) only a tiny Fe^{3+} doublet is observed corresponding to the very small amount of corrosion products found on the steel surface (SEM images, Fig. 3 (right)). In the case of the 0.04 vol% atmosphere, the CEMS spectrum is dominated by intense Fe^{3+} contributions while only additional small Fe^{2+} doublets are observed. Finally, when weathering steel is exposed to an atmosphere containing a high SO_2 concentration (0.22 vol%), the most intense contributions to the CEMS spectrum correspond by far to the Fe^{2+} species, the Fe^{3+} species representing only a very small percentage. In all the cases, the peaks from the substrate can be observed indicating that the corrosion layers formed at this exposure time are thin enough as to allow the conversion electrons from the substrate to pass through the corrosion layer and be detected. However, it is clear that the area of the substrate peaks decrease with increasing SO_2 concentration. So, it can be concluded that higher SO_2 concentrations promote, for the same corrosion time, both a thicker layer of corrosion products and a higher concentration of Fe^{2+} species. The SO_2 concentration has also a clear influence on the morphology of the rust layer and in the way that corrosion proceeds at the very early stages of the corrosion process. It seems that initially corrosion starts in localized points of the surface at specific adsorption points (it is known that a high relative humidity, as is the case here, facilitates SO_2 adsorption) where small water droplets can also condensate. These droplets can coalesce until forming a more continuous film where O_2 and SO_2 are dissolved giving place to a continuous acid electrolyte layer on the metal surface. This process appears to be accelerated with increasing SO_2 concentration. In this acid electrolyte the anodic dissolution of iron



takes place. Then, depending on the local conditions, Fe^{2+} compounds (in our case $\text{FeSO}_3 \cdot 3\text{H}_2\text{O}$ and an Fe^{2+} thiosulphate/tetrathionate) can precipitate. These ferrous species can be oxidized in their outer surface to an Fe^{3+} species which has Mössbauer parameters ($\delta = 0.38$

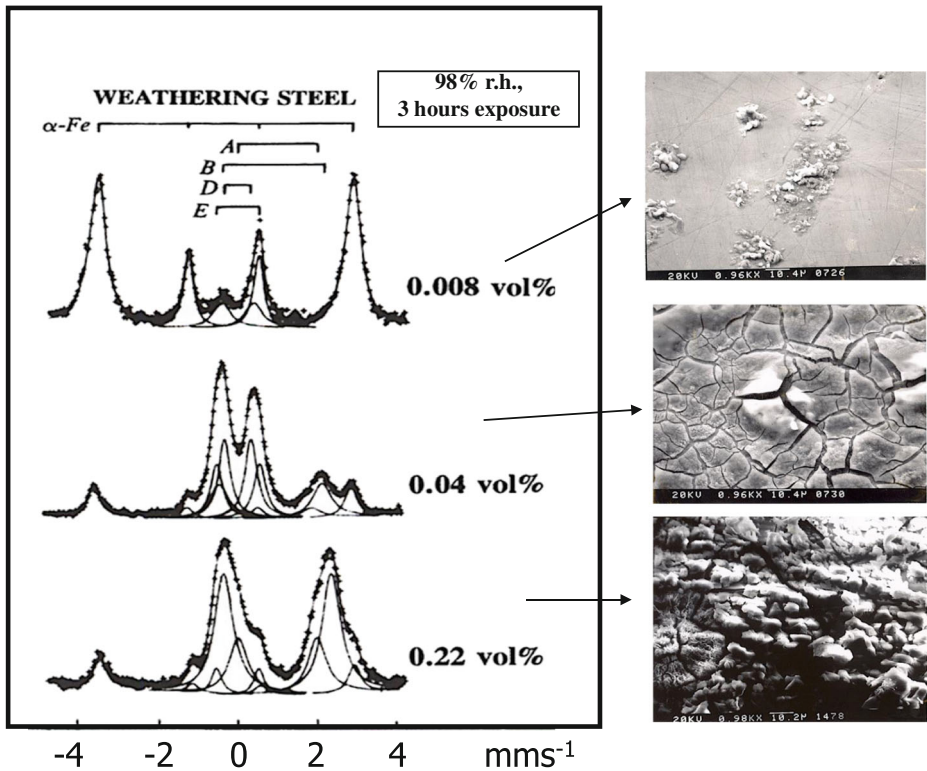


Fig. 3 *Left:* CEMS spectra recorded from weathering steel exposed for 3 hours to an atmosphere with 98% rh and different SO₂ concentrations. *Right:* SEM images from the corresponding samples on the left

mms⁻¹; $\Delta = 1.08 \text{ mms}^{-1}$) characteristic of a gel-like amorphous ferric oxyhydroxide [27, 28] (we will come to this point later). The only presence of Fe³⁺ compounds in the atmosphere with the lowest SO₂ concentration might be due to the fact that at moderate pH's the solubility of Fe³⁺ compounds is lower than that of Fe²⁺ compounds.

3.2.2 Influence of the exposure time

Figure 4 (left) shows the evolution of the Mössbauer spectra recorded after different exposure times from weathering steel subjected to a SO₂-polluted atmosphere containing 0.04 vol% SO₂ and 98% relative humidity. On the right side SEM images taken at selected exposure times are presented. As it can be deduced from Fig. 4, as corrosion time increases the peaks from the substrate decrease, i.e., the corrosion layer increases in thickness and the initially predominant Fe²⁺ phases are oxidized to Fe³⁺ phases. It is also important to note that the lines of the doublets corresponding to the Fe³⁺ phases formed after 72 hours of exposure are less broad ($\sim 0.34 \text{ mms}^{-1}$) than those of the doublets recorded at shorter times ($\sim 0.38\text{--}0.40 \text{ mms}^{-1}$) what suggests that the corrosion products formed at longer exposure times present a higher degree of crystallinity/larger particle size. The predominant Fe³⁺ doublet at this corrosion time is that with parameters ($\delta = 0.38 \text{ mms}^{-1}$; $\Delta = 0.67 \text{ mms}^{-1}$) which are close to those of superparamagnetic $\alpha\text{-FeOOH}$ [25]. This spectrum still shows an Fe³⁺

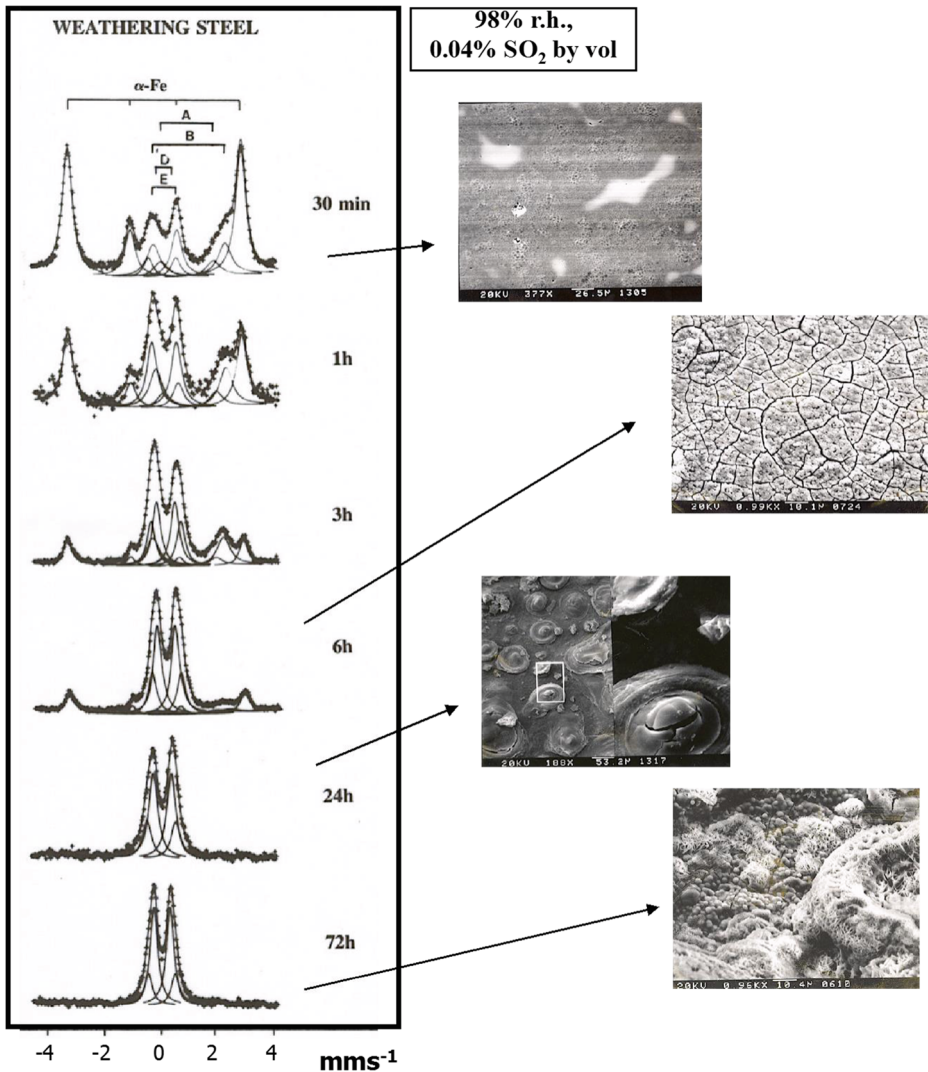


Fig. 4 *Left*: CEMS spectra recorded from weathering steel exposed for different times to an atmosphere with 98% rh and 0.04 vol% SO₂. *Right*: SEM images from the corresponding samples on the left

doublet with a larger quadrupole splitting indicating that the composition of the corrosion scale can be complex as we will show later.

The evolution of the morphology of the corrosion layer reveals interesting details (Fig. 4, right). At very short exposure times (30 min) the surface is not completely covered indicating, as mentioned in the above section, that corrosion starts at localized sites. At the intermediate time of 6h, the steel surface is already completely covered by a layer of corrosion products. The layer contains many cracks and has a quite structureless appearance except for a few protuberances here and there. After 24 hours, multiple “pustules” having a very characteristic shape cover the surface: a circular valley surrounds a central protuberance and after those a circular ring is observed (see the area within the marked box in

the corresponding image). These pustules are a clear example of what in the literature are known as “sulphate nests” [29]. A sulphate nest is a reservoir of electrolyte rich in SO_4^{2-} and Fe^{2+} ions covered by an amorphous ferric oxyhydroxide layer which acts as a membrane and that prevents the sulphates contained inside from further oxidation. At some stages of the process this membrane can break due to inner osmotic forces and the contents of the nest can be spread activating another corrosion center. In our case, in view of the Mössbauer spectra, it could be more appropriate to call these features “sulphite nests” as it is ferrous sulphite the main sulphur-containing species in these corrosion layers. Although ferrous sulphite is unstable and oxidizes readily in solution a large SO_2 concentration can stabilize it [22]. Besides this, the existence of a Fe^{3+} membrane gel-like can preserve it temporary from oxidation. Since this membrane limits the passage of water and oxygen into the nests, the crystallization of $\text{FeSO}_3 \cdot \text{H}_2\text{O}$ can be allowed. At some stage, when the local conditions are favourable (for example if the SO_2 concentration is not too high and then the pH inside the nest is just moderate or if, at higher SO_2 concentrations, the exposure time has been long enough as to allow a sufficient passage of oxygen into the nests) the oxidation of Fe^{2+} to Fe^{3+} can occur and the growth of the Fe^{3+} species can cause finally the breakage of the membrane giving place to the formation of the small acicular crystals observed in the SEM image at the right (bottom) of Fig. 4. The presence of these acicular microcrystals support the Mössbauer observations since these type of shape is often shown by α - FeOOH microcrystals [30, 31] and it is obvious from the SEM images of Fig. 4 that the compounds formed after 72h present a higher degree of crystallinity than those formed at shorter corrosion times. The images also show a noticeable number of spherical particles that can be due to a different phase (probably ferrihydrite) indicating the complex composition of the corrosion layer.

3.2.3 Nature of the Fe^{3+} species formed after “long” exposure times to atmospheres with constant rh

A key point to understand the protective character of the patina formed on weathering steels is to determine its composition in samples that have been subjected to long exposure times to the corrosive atmosphere. Under some accelerated laboratory conditions (a few days) the appearance, thickness and other macroscopic characteristics of the corrosion layers are very similar to those found in weathering steels exposed for long periods (months/years) to natural environments, when their protective effect has been sufficiently demonstrated. Under these laboratory conditions, the corrosion layer is thick enough as to be scraped from the metal surface and, thus, be studied by transmission Mössbauer spectroscopy. As we have mentioned before, a room temperature Mössbauer spectrum is relatively unspecific as several Fe^{3+} oxyhydroxides can give, even more if they are in a superparamagnetic state, a very similar spectrum. In fact, X-ray diffractograms (not presented) showed a few broad, not well-defined bands at the d-spacings 2.24 Å (which matches the most intense diffraction line of goethite), 2.5 Å and 1.5 Å (which can be associated to ferrihydrite) and a weak one at 6.14 Å which is characteristic of lepidocrocite. Therefore, low temperature measurements become compulsory to elucidate the nature of that patina.

Figure 5 (left) shows the transmission Mössbauer spectra recorded at three different temperatures from the corrosion layer formed on weathering steel after 72 h of exposure to a SO_2 -polluted atmosphere containing 0.04 vol% SO_2 and 98% rh. An intense Fe^{3+} doublet dominates the room temperature spectrum accompanied by a less intense broad magnetic component characterized by a hyperfine magnetic field close to 35.0 T. We associate this magnetic component with a fraction of goethite [25] particles with a size large enough as

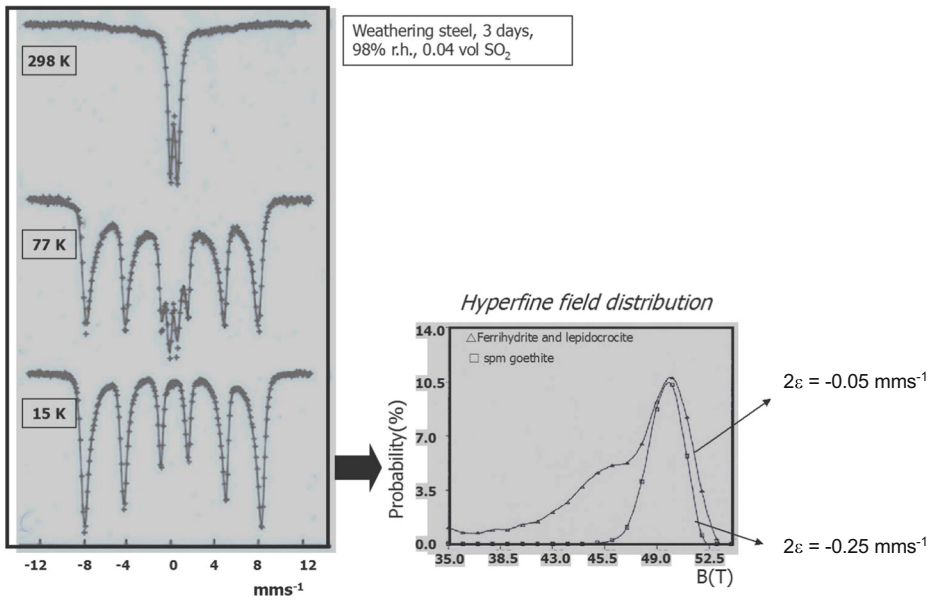


Fig. 5 *Left*: Transmission Mössbauer spectra recorded at different temperatures from the corrosion layer formed on weathering steel after 3 days of exposure to an atmosphere with 98% rh and 0.04 vol% SO₂. *Right*: Hyperfine magnetic field distributions used to fit the 15 K spectrum

to give a magnetic spectrum at room temperature but small enough as not to be that characteristic of well-crystallized goethite. Superparamagnetic effects are evident. The spectrum recorded at 77 K still shows the presence of a doublet together with a quite intense magnetic component having very asymmetric lines characteristic of a particle size distribution. We assume that goethite is contributing significantly to that magnetic component, although the presence of other oxyhydroxides, as for example ferrihydrate, cannot be discarded. This statement is based on the values of the hyperfine parameters obtained from the fit of such magnetic component to a hyperfine field distribution: $\delta = 0.45 \text{ mms}^{-1}$; $2\epsilon = -0.12 \text{ mms}^{-1}$ and $H_{\text{max}} = 48.0 \text{ T}$. The 2ϵ value lies between that of goethite (typical values are around -0.25 mms^{-1}) and that of ferrihydrate (-0.05 mms^{-1}) [25]. Thus, more likely, this intermediate value represents a situation in which a mixture of goethite and ferrihydrate is present. It is worth noting here that the magnetic ordering temperature of lepidocrocite is around 52 K [32], therefore this phase can be also contributing to the observed doublet at 77 K. The spectrum recorded at 15 K shows a very well developed magnetic pattern although with asymmetric lines indicating that a particle size distribution and/or more than one phase is present. If this spectrum is fitted considering only one hyperfine magnetic field distribution we obtain parameters similar to those obtained for the 77 K magnetic component. At 15 K the hyperfine magnetic fields of goethite and ferrihydrate are similar (50.0 T) while that of lepidocrocite is much lower (45.8 T). Besides this, the 2ϵ value of ferrihydrate and lepidocrocite are about the same (-0.05 mms^{-1}), that of goethite being, as mentioned above, -0.25 mms^{-1} . Therefore, we have tried a fitting procedure aimed to disentangle, if possible, the contributions from these three phases. In this fitting procedure we used two hyperfine magnetic field distributions with fixed 2ϵ values: -0.05 mms^{-1} to account for ferrihydrate/lepidocrocite and -0.25 mms^{-1} to account for goethite. The obtained distributions are

shown in the bottom right side of Fig. 5. As it can be observed the distribution corresponding to goethite is quite narrow (~ 2.6 T) and symmetrical. This is consistent with the SEM images discussed above where well-defined goethite crystallites were observed. The other distribution is much broader (~ 4.5 T). It peaks also at 50.0 T (value typical of ferrihydrite) and has a clear shoulder at 46.0 T, the characteristic hyperfine magnetic field of lepidocrocite. Therefore, the results indicate that after “long” exposure times the corrosion layer is mainly composed by goethite and ferrihydrite with a smaller concentration of lepidocrocite. Recent works [13] claim that nanosized goethite is the main responsible for the protective effect of the patina formed on weathering steels in natural environments. Our results indicate that, in this type of laboratory experiments, superparamagnetic goethite is one of the main constituents of the “old” rust but it is undeniable that ferrihydrite also plays an important role whilst lepidocrocite appears only to play a marginal one despite the fact that the latter is a very common corrosion product in natural environments [13, 15]. It is known that the formation of goethite is favoured over the formation of lepidocrocite if the $[\text{Fe}^{2+}]/[\text{Fe}^{3+}]$ ratio in the precursor sulphate solutions is large [33]. This is the situation here since Fe^{2+} is rarely encountered in large quantities in field corrosion studies of this type of steels, probably because the SO_2 concentrations are smaller.

3.2.4 Effect of exposure to wet-dry cycles

The influence that the exposure of the steels to wet-dry cycles has on the composition of the corrosion layer was also investigated since they appear to be beneficial to develop a protective patina [11, 34]. The succession of wet-dry cycles is a way of simulating the alternative humidity/dryness periods that take place in natural environments. As an example, Fig. 6 shows the spectra recorded from weathering steel surfaces exposed to an atmosphere containing 0.04 vol% SO_2 with either a constant relative humidity of 98% (top left) or subjected to SW wet-dry cycles (top right). If we compare the results obtained after exposure for one day to the constant rh atmosphere with those obtained after exposure to four SW wet-dry cycles (note that exposure to four SW cycles implies that the samples have been subjected to one day of 98% rh but in periods of 6h separated by dry periods of 18 h) very different spectra are obtained. In the first case, the CEMS spectrum only shows Fe^{3+} components whilst in the second a very substantial amount of Fe^{2+} phases is still present in the rust layer. Even more, a tiny contribution from the steel substrate can be observed in the samples corroded during the SW experiments indicating that the corrosion layer formed under these conditions is much thinner than under constant rh conditions. The situation is maintained even for longer exposure times (see Fig. 6, top): the amount of Fe^{2+} has decreased only slightly after 18 cycles. It appears, then, that wet-dry cycling conditions delay considerably the transformation of Fe^{2+} into Fe^{3+} species as compared with that occurring under corrosion in constant rh atmospheres.

Besides hindering Fe^{2+} oxidation, wet-dry cycling influences very much the nature of the Fe^{3+} species formed after long exposure times. Figure 6 shows that the Fe^{3+} phases formed after 24 SW cycles do not give a magnetic ordered spectrum at 15 K in contrast with that formed after 3d in 98% rh where, as explained in detail in the above section, a spectrum with a very well defined magnetic pattern is observed. Note again that 24 SW cycles mean that the samples have been subjected for 6 days at a 98% rh in periods of 6h with dry periods in between. That is, in this particular case, they have been subjected to 98% rh a time twice longer than the samples that have suffered an uninterrupted continuous exposure. The absence of magnetic order in the spectra of the cycled samples indicates that the Fe^{3+} phases formed even after a large number of cycles are either very poorly crystalline

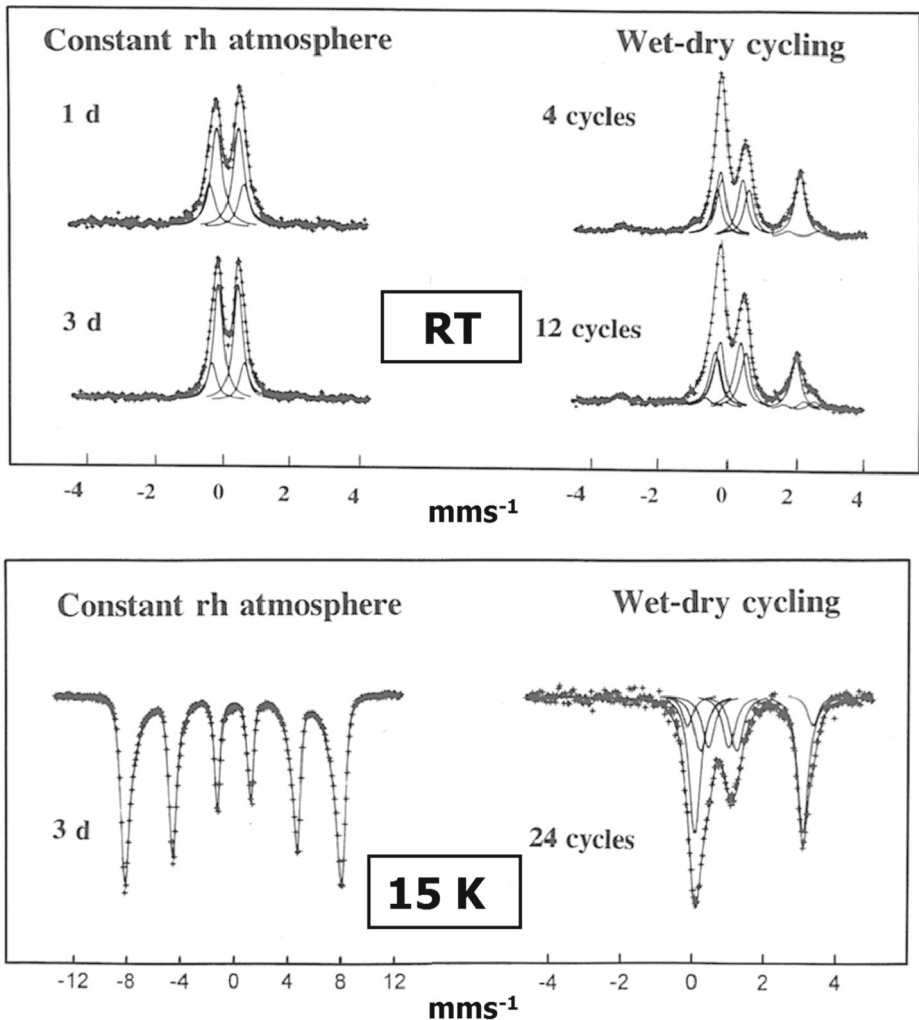


Fig. 6 *Top*: Room temperature CEMS spectra recorded from weathering steel exposed to an atmosphere containing 0.04 vol% SO₂ under either constant rh (98%) or wet-dry cycles (SW). The duration of the exposure is indicated in the Figure. *Bottom*: 15 K spectra recorded from the corrosion layer formed under the conditions indicated in the Figure in a 0.04 vol% SO₂ atmosphere

or of an extremely small particle size. Macroscopically, these layers result to be much more adherent than those formed under constant humidity.

The situation changes if LW cycles are considered. The corrosion rate under LW conditions estimated by weight gain measurements is much higher than under SW conditions (Fig. 7). Obviously, the conditions under LW cycles are closer to those occurring under constant rh exposure.

It is clear that the effect of the dry period is to stabilize the Fe²⁺ species, whose oxidation by the O₂ dissolved in the aqueous film formed during the wet period takes place more easily than when they have already precipitated during the dry period due to the disappearance of this water film. The changes in the thickness of this water film,

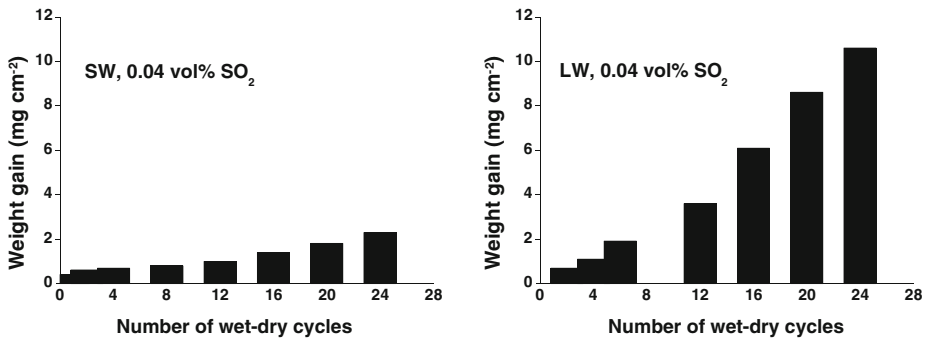


Fig. 7 Weight gains measured on weathering steel exposed to an 0.04 vol% SO₂ atmosphere under SW and LW type-cycles

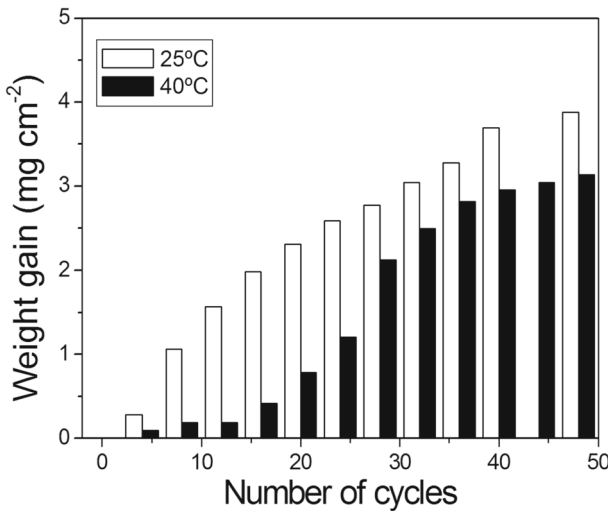


Fig. 8 Weight gains measured on weathering steel exposed to an 0.001 vol% SO₂ atmosphere under SW type-cycles with different temperature of the dry period

together with the concomitant variations in the solutes concentration (i.e. the occurrence of a precipitation-redissolution mechanism) would be the responsible for the poorly crystalline character/small particle size of the Fe³⁺ formed under these corrosion conditions and for the delay in the formation of the goethite microcrystals observed in the constant rh atmospheres.

3.2.5 Influence of the rise a temperature during the dry period

Early corrosion studies [35, 36] suggested that the rise of the temperature during the dry period in natural environments could be beneficial to slow the corrosion process. Our weight gain results (Fig. 8) clearly indicate that the corrosion rate of weathering steels decreases significantly when the temperature of the dry period rises from 25 °C to 40 °C, specially when the number of wet-dry cycles is low. For a larger number of cycles the differences

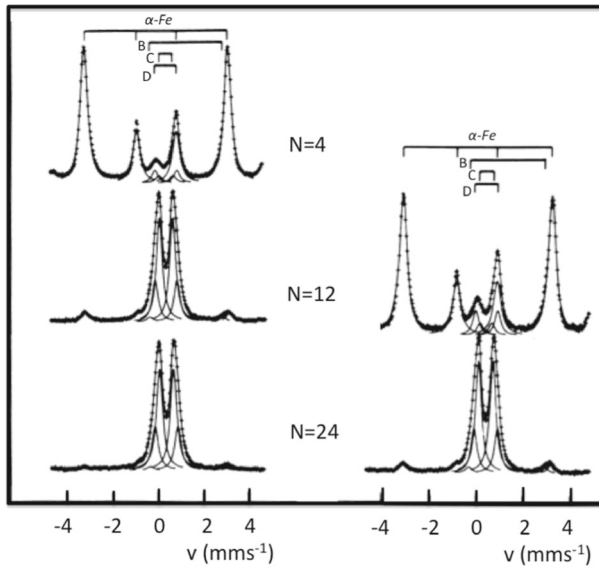


Fig. 9 CEMS spectra recorded under SW cycles in a 0.001 vol% SO₂ atmosphere (N=number of cycles). Temperature during the dry period: 25 °C (left) and 40 °C (right)

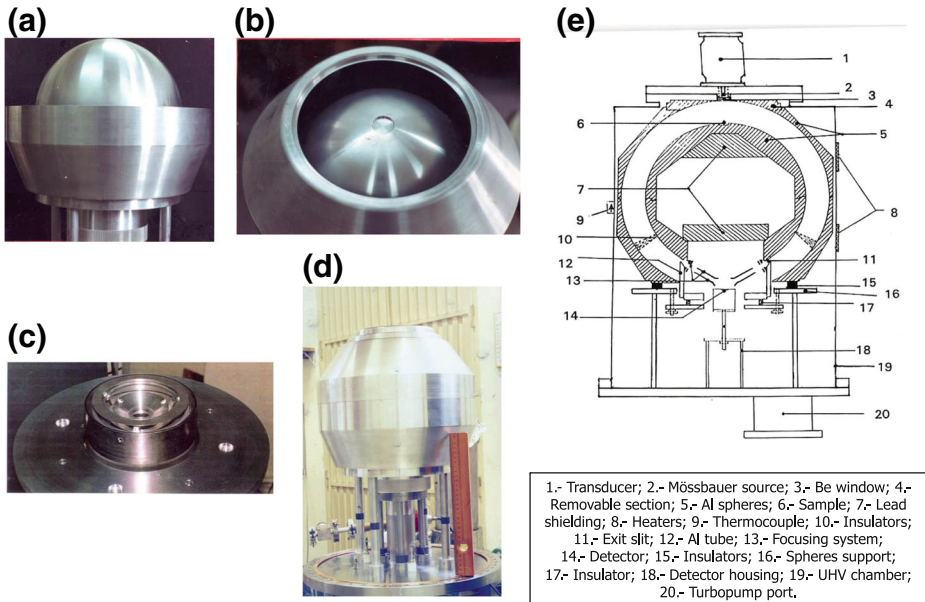


Fig. 10 a–d Different views of the spherical electron analyser for DCEMS built by the authors (the vacuum chamber was removed to take the photos). e Schematic cross section showing the different parts of the analyser

in weight gains decrease but, in any case, they are smaller for the samples corroded under conditions in which the ambient temperature during the dry period rises to 40 °C.

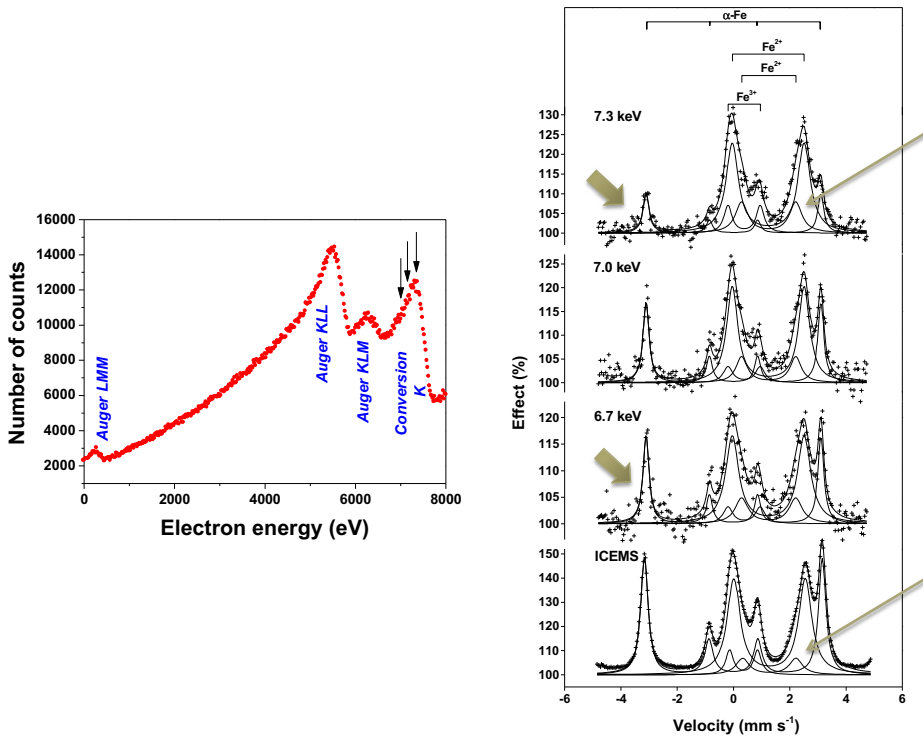


Fig. 11 ICEMS and DCEMS spectra recorded at various energies in the 7.3 keV K-conversion electrons edge (see the corresponding arrows in the electron spectrum on the left) from a sample exposed for 4h to an atmosphere with 98% rh and 0.22 vol% SO₂. The broad arrows in the spectra on the right point to the α -Fe peaks to show their intensity reduction with increasing electron energy. The narrower lines point to the Fe^{2+} doublet corresponding to the Fe^{2+} dithionate/thiosulphate species to show its intensity increase with increasing electron energy

This is also reflected in the CEMS spectra (Fig. 9). If the temperature of the dry cycle is 40 °C, the spectra start showing the evidence of the presence of corrosion products after 12 cycles and only in a very small concentration. From the point of view of the CEMS results there is no difference at 24 cycles.

3.2.6 Spatial distribution of the corrosion species

Early corrosion stages We built a spherical electrostatic analyser (Fig. 10) to study the spatial distribution of the corrosion phases at the very early stages of the corrosion process when the thickness of the corrosion layer is still very thin, within the nanometer scale, and under conditions that give place to abundant Fe^{2+} species. Figure 11 shows a series of spectra recorded from a sample corroded for 4 h (0.22 vol% SO₂, 98 % rh). The bottom spectrum presents the corresponding Integral CEMS spectrum, which shows the usual corrosion species formed under these conditions and that have been commented above. The rest of spectra were recorded at different energies in the edge of the 7.3 keV conversion electrons (indicated by arrows in the electron spectrum on the left of Fig. 11). The main difference among the spectra is the dramatic increase in the peaks corresponding to the metal substrate

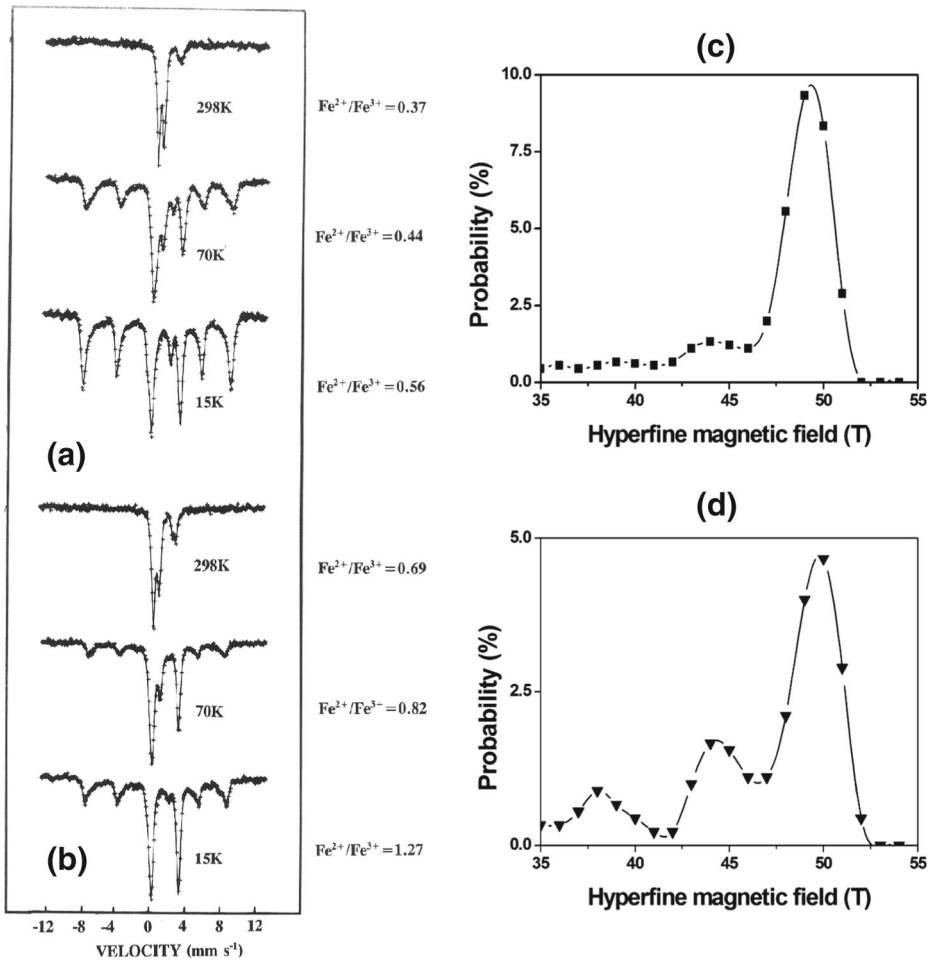


Fig. 12 Transmission Mössbauer spectra recorded at different temperatures from (a) the outer layer (b) the inner layer of corrosion products of a sample exposed for 3d to a 98% rh atmosphere containing 0.22 vol% SO₂. The different Fe²⁺/Fe³⁺ ratios calculated from the spectra are shown. c and d: Hyperfine magnetic field distributions used to fit the 15 K spectra on the left

as the selected electron energy decreases. This is a clear indication of the right operation of the analyser: we detect a smaller contribution from the substrate when we record data from electrons without energy loss. The evolution of the corrosion species is not so clear, although the data suggest (see arrows on the right side of Fig. 11) that the doublet due to the Fe²⁺ thiosulphate/tetrathionate has a larger area in the spectrum recorded at $E_{el} = 7.3$ keV. This would imply that this species would be located towards the upper part of the corrosion layer. Therefore it could be more easily oxidized than ferrous sulphite what would explain why it disappears earlier from the corrosion layer.

Advanced corrosion stages After long exposure times the corrosion scale always presents a double layer structure: a very loosely outer part that descales very easily and a

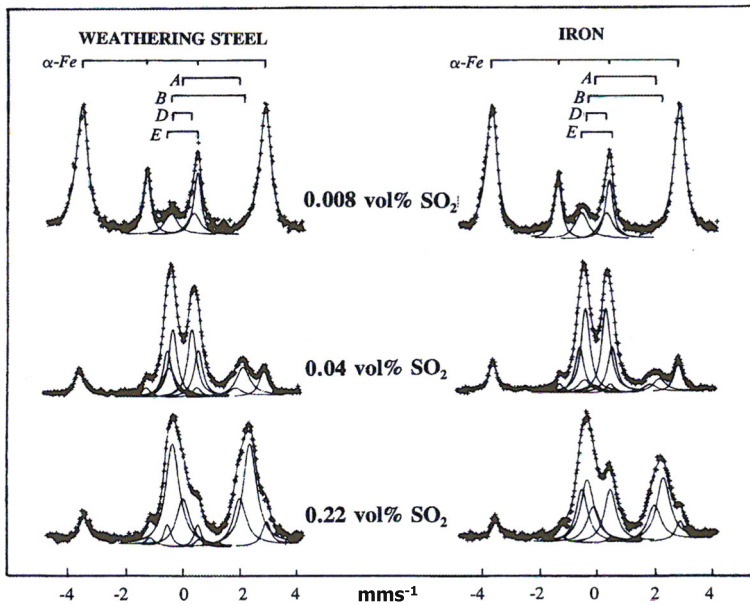


Fig. 13 CEMS Mössbauer spectra recorded from weathering steel and pure iron after 3d of exposure to atmospheres containing different SO₂ concentrations and 98% rh

very adherent inner part which is very difficult to scrape out of the metal. For high SO₂ concentrations the inner layer is significantly much richer in Fe²⁺ phases than the outer layer (Fig. 12, a-b). In fact, the 15 K data demonstrate that the concentration of Fe²⁺ phases is much larger (almost double) than that suggested by the room temperature spectra because of the very large difference in the respective recoil free fractions of the Fe³⁺ and Fe²⁺ compounds at 298 K.

Another important and general fact, as it occurs for all the experimental conditions examined, is that the Fe³⁺ compounds located in the inner layer have a much smaller particle size/degree of crystallinity than those of the outer layer. This is confirmed by the low temperature data. If we consider the hyperfine field magnetic distributions used to fit the magnetic part of the 15 K spectra shown in Fig. 13 (Fig. 13, c-d) we see that they both peak at about 50 T but that the contribution of smaller fields is much more important in the case of the inner layer than in the case of the outer layer, what is consistent with the statement made a few lines above.

3.2.7 Importance of alloying

Finally we will show in this paper the differences in corrosion behaviour among weathering steels and pure iron to exemplify the importance of the alloying elements.

Generally speaking, for the same exposure time or the same number of wet-dry cycles, the corrosion rate, as shown by weight gains (not presented), is much higher in pure iron than in weathering steel. Also, the concentration of Fe²⁺ species is always lower in pure iron than in weathering steel (Fig. 13) what indicates that the transformation of Fe²⁺ compounds into Fe³⁺ occurs more slowly in weathering steel than in pure iron. As it was reported long ago [37], minute concentrations of Cu²⁺ (alloying element which is present in weathering

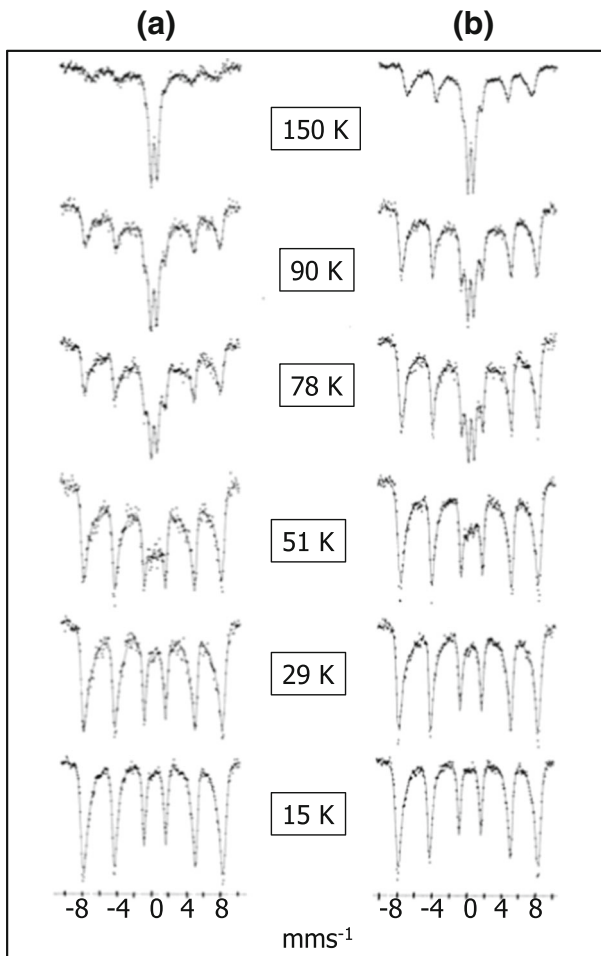


Fig. 14 Transmission Mössbauer spectra recorded at different temperatures from the corrosion layer formed on weathering steel and pure iron after 3d of exposure to an atmosphere containing 0.04 vol% SO₂ and 98% rh

steel) can inhibit the oxidation of sulphite what would explain the prevalence of ferrous sulphite in the corrosion layer of this material.

As discussed before, the nature of the Fe³⁺ formed after long exposure times is key to understand the behaviour of the protective patina formed on weathering steels. As Fig. 14 shows, both the corrosion layer formed on weathering steel and pure iron have a markedly superparamagnetic behaviour: the coexistence of a doublet and a magnetic pattern takes place over a very large temperature interval (from 298 K to 50 K). However, at any given temperature between 298 K and 50 K the doublet is considerably more intense in the spectra recorded from weathering steel than in those recorded from pure iron. If we assume, as commented in the previous sections, that ferrihydrite, goethite and a small proportion of lepidocrocite mainly compose the rust formed at these stages, the results indicate that the rust on weathering steel contains a larger concentration of ferrihydrite or goethite with smaller

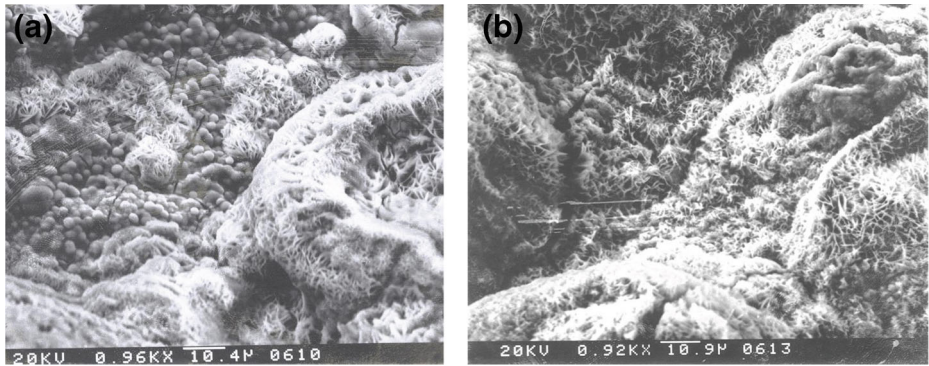


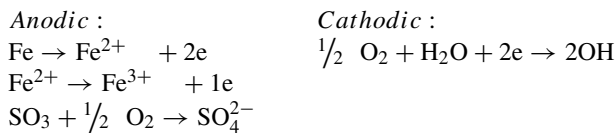
Fig. 15 SEM images recorded from the corrosion layer formed on (a) weathering steel and (b) pure iron after 3d of exposure to an atmosphere containing 0.04 vol% SO₂ and 98% rh

particle size than that of pure iron. In fact SEM images recorded from these layers (Fig. 15) show a much larger number of acicular crystals (characteristic of goethite) and almost the total absence of spherical particles (probably ferrihydrite) in the rust of iron. Clearly, this difference in paramagnetic behaviour has to be related to the presence of alloying elements in particular Cu and Cr, and much discussion has taken place in the literature to understand their particular roles [10, 13, 38, 39]. Very early investigations proved that minute concentrations of Cu²⁺ hinder the precipitation and crystal growth of goethite from acid solutions [40]. Although we have no direct proof that this mechanism is occurring here we can think seriously in its plausibility.

4 Summary and final considerations

Although the main mechanisms underlying the results observed here have been outlined briefly in the various sections along the paper, we would like to finish it giving a complete overview of them.

So, in the atmospheres having a high constant relative humidity during all the corrosion time, a film of water is formed at the beginning of the exposure on the surface of the metals where O₂ and SO₂ are dissolved giving place to the formation of an acid electrolyte medium. In this electrolyte the following reactions occur:



Depending on the local conditions (pH, O₂ concentration, solutes concentration) different compounds can precipitate. Ferrous sulphite and an Fe²⁺ thiosulphate/tetrathionate are the most abundant ferrous phases. Fe³⁺ oxyhydroxides can precipitate but if the medium is very acid, as at the beginning of the exposure, they can be redissolved and reduced to Fe²⁺ giving place to another anodic path. When the acidity decreases, the crystallites of Fe³⁺ oxyhydroxides grow incorporating Fe³⁺ from solution, the nucleation taking place over initially formed crystallites. Cu²⁺ however, can inhibit this growth. As corrosion time

increases, SO_3^{2-} is oxidized to SO_4^{2-} (a reaction which is also inhibited by the presence of Cu^{2+}) while Fe^{2+} is oxidized to Fe^{3+} mainly in the outer part of the corrosion layer.

In the case of wet-dry cycles, the situation in the first wet period is the same than that occurring in the case of constant humid atmospheres. At the beginning of the dry period the thickness of the water film decreases facilitating the diffusion of O_2 , increasing its cathodic reduction and, therefore, favouring the attack of the bare metal and the partial oxidation of Fe^{2+} and SO_3^{2-} . Besides, oxyhydroxide gels constituting the membrane that covers sulphite/sulphate nests dry. The nests burst and their contents are released. Under the conditions used, this happens in a short time as compared to the total exposure time. When the dry period is consolidated corrosion stops because the electrolyte cell cannot work without a solvent and the soluble Fe^{2+} products precipitate. At the beginning of the next wet period redissolution occurs, soluble Fe^{2+} compounds are dissolved and because of the acidity of the medium the Fe^{3+} compounds formed in the preceding cycle can be redissolved and reduced to Fe^{2+} . Then, the mechanisms occurring during the wet period take place again. Because of the occurrence of repeated dissolution/precipitation mechanisms, cycling favours both the permanence of Fe^{2+} compounds and of finely divided rust.

Recent investigations and reviews on the protectiveness of the patina developed in natural environments have reported that it is due to nanosized goethite [13, 14]. This would be predominantly located in the inner part of the corrosion layer while lepidocrocite would be the main constituent of the outer layer [13]. Depending on the corrosion conditions (presence of other pollutants) or exposure time, maghemite can be also formed [41]. The influence of wet-dry cycles has shown to be beneficial: more protective layers are formed under wet-dry conditions [11, 34] while very long exposure to humid periods results in poorly adherent layers and in the lack of protective character [13], as we have also found here. In general not too much mention of the role of ferrihydrite is found in the relevant literature although we have shown here that in these experiments it takes an important role.

We must say that corrosion by SO_2 is obviously a very complex matter and that results presented here have been obtained under accelerated corrosion tests using extreme conditions of humidity and SO_2 contamination. Therefore, these experiments help in understanding mechanisms but, anyway, they are laboratory simulations that must be considered as a complement to the very necessary field experiments.

Acknowledgments The author would like to acknowledge the work of Drs. J.R. Gancedo, M. Gracia, J. Palacios, J.Z. Dávalos, W. Meisel and J.A. Tabares who contribute strongly to obtain the results reported in this paper. Financial support from different instances of the Spanish Administration and the CSIC is also acknowledged.

References

1. Uhlig, H.H.: Corrosion and corrosion protection, 2nd edn. Wiley, USA (1971)
2. Koch, G., Varney, J., Thompson, N., Moghissi, O., Gould, M., Payer, J.: International measures of prevention, application and economics of corrosion technologies study NACE International, vol. 15385. USA, Park Ten Place (2016)
3. Smith, S.J., van Ardenne, J., Klimont, Z., Andres, R.J., Volke, A., Arias, S.d.: Atmos. Chem. Phys. **11**, 1101 (2011)
4. Pourbaix, M.: Atlas of electrochemical equilibria in aqueous solutions, 2nd edn. NACE, USA (1974)
5. Leidheiser, H. Jr., Simmons, G.W., Kellerman, E.: Croat. Chem. Acta **45**, 257 (1973)
6. Meisel, W.: J. Phys. Coll. (Paris) CI **41**, 63 (1980)
7. Meisel, W.: Hyp. Int. **45**, 73 (1989)
8. Vèrtes, A., Czako-Nagy, I.: Electrochim. Acta **34**, 721 (1989)

9. Marco, J.F., Dávalos, J., Gracia, M., Gancedo, J.R.: *Hyp. Int.* **83**, 111 (1994)
10. Pourbaix, M., Pourbaix, A.: *CEBELCOR, Rapp. Techn.*, 141 (1967)
11. Morcillo, M., Chico, B., Diaz, I., Cano, H., De la Fuente, D.: *Corros. Sci.* **77**, 6 (2013)
12. Misawa, T., Asami, K., Hashimoto, K.Y., Shimodaira, S.: *Corros. Sci.* **14**, 279–289 (1974)
13. Oh, S.J., Cook, D.C., Townsend, H.E.: *Corros. Sci.* **41**, 1687–1702 (1999)
14. Chiavari, C., Bernardi, E., Martini, C., Passarini, F., Motori, A., Bignozzi, M.C.: *Mat. Chyem. Phys.* **136**, 477–486 (2012)
15. Cook, D.: *Hyp. Int.* **153**, 61 (2004)
16. Evans, U.R., Taylor, C.A.J.: *Corros. Sci.* **12**, 227 (1972)
17. Gancedo, J.R., Gracia, M., Marco, J.F.: *Hyp. Int.* **83**, 71–78 (1994)
18. Gancedo, J.R., Gracia, M., Marco, J.F.: *Hyp. Int.* **66**, 83 (1991)
19. Gracia, M., Marco, J.F., Gancedo, J.R., Exel, W., Meisel, W.: *Surf. Interf. Anal.* **29**, 82 (2000)
20. Strandberg, H., Johanson, L.-G.: *J. Electrochem. Soc.* **144**, 81 (1997). and references therein
21. Abraham, K.M., Chaudri, S.M.: *J. Electrochem. Soc.* **133**, 1307 (1986)
22. Bugli, G., Pannetier, G.: *Bull. Soc. Chim. Fr.*, 2355 (1968)
23. Murad, E.: *Amer. Miner.* **67**, 1007 (1982)
24. Murad, E., Schwertmann, U.: *Miner. Mag.* **48**, 507 (1984)
25. Murad, E., Johnston, H.: *Mössbauer Spectroscopy Applied to Inorganic Chemistry*. In: Long, G.J. (ed.), vol. 2, pp. 507–582. Plenum Pub. Co., New York-London (1987)
26. Murad, E.: *Iron in soils and clay minerals*. In Stucki, J.W. (ed.), pp. 309–350. D. Reidel Pub. Co (1988)
27. Murad, E., Schwertmann, U.: *Amer. Miner.* **65**, 1044 (1980)
28. Brett, M.E., Parkin, K.M., Graham, M.J.: *J. Electrochem. Soc.* **133**, 2031 (1986)
29. Graedel, T.E., Frankenthal, R.P.: *J. Electrochem. Soc.* **137**, 2385 (1980)
30. Raman, A., Razvan, A., Kuban, B., Clement, K.A., Graves, W.E.: *Corrosion* **42**, 447 (1986)
31. Razvan, A., Raman, A.: *Pract. Met.* **23**, 223 (1986)
32. Hirt, A.M., Lanci, L., Dobson, J., Weidler, P., Gehring, A.U.: *J. Geophys. Res.* **107**, EPM5-1 (2002)
33. Music, S., Czako-Nagy, I., Popovic, I., Vêrtes, A., Tonkovic, M.: *Croat. Chem. Phys.* **66**, 5798 (1977)
34. Stratmann, M.: *Corros. Sci.* **27**, 869 (1987)
35. Pourbaix, M.: *Corros. Sci.* **14**, 25 (1974)
36. De Miranda, L.: *CEBELCOR, Rapp. Techn.* **217** (1974)
37. Bennet, H., Parker, W.G.: *J. Chem. Soc.*, 1540 (1951)
38. Inouye, K.: *J. Colloid Interf. Sci.* **27**, 171 (1998)
39. Kanimura, T., Hara, S., Miguki, H., Yamashita, M., Uchida, N.: *Corros. Sci.* **48**, 2799 (2006)
40. Inouye, K., Ishii, S., Kaneko, K., Ishikawa, T.: *Z. anorg. Allg. Chem.* **391**, 86 (1972)
41. Chico, B., Alcántara, J., Pino, E., Díaz, I., Simancas, J., Torres-Pardo, A., de la Fuente, D., Jiménez, J.A., Marco, J.F., González-Calbet, J.M., Morcillo, M.: *Corros. Rev.* **33**, 263 (2015)